Detection of blood in fish muscle by constrained spectral unmixing of hyperspectral images

Martin H. Skjelvareid [a] *, Karsten Heia [a], Stein Harris Olsen [a] & Svein Kristian Stormo [a]

* Corresponding author. E-mail: *mhs@nofima.no*
[a] Department of seafood industry, Nofima AS, P.O. Box 6122, 9291 Tromsø, Norway

Abstract

A new method for blood detection in whitefish fillets is presented. The method is based on diffuse reflectance hyperspectral imaging in the VIS/NIR range, and unmixing of measured absorbance spectra into known spectra for hemoglobin, water and muscle tissue. Scattering effects are modelled as a polynomial function of wavelength, and are included in the unmixing procedure. The unmixing method is based on a modified Beer-Lambert law and is performed using a non-negativity constrained least squares algorithm. Application of the method to images of samples with varying amounts of blood results in a very good fit between measured and modelled spectra. Reference measurements on homogenized cod muscle with controlled concentrations of added blood are used to model the relationship between the spectral unmixing results and hemoglobin concentration, enabling pixel-by-pixel estimation of hemoglobin concentration. The method is seen as a useful tool for automatic quality grading and processing of fillets in the whitefish industry.

Keywords: hyperspectral imaging, spectral unmixing, fish, cod, fillet, blood

1 INTRODUCTION

Hyperspectral imaging (HSI) is a combination of two measurement techniques, imaging and spectroscopy, which produces images where each pixel contains detailed spectral information. Light interacting with different types of material is absorbed and/or scattered at characteristic wavelengths depending on the materials' composition and structure. Spectral information from HSI can therefore be used to determine the composition of the imaged material, or to distinguish between different types of material. A typical application is remote sensing, where the spectral information is used to classify different types of terrain and vegetation (Keshava, 2003; Thenkabail et al., 2011; van der Meer et al., 2012). Other applications include medical imaging (Lu and Fei, 2014), mineralogy (Kruse, 1996) and food quality control (Elmasry et al., 2012; Gowen et al., 2007).

In the field of food quality control, spectral information is used for measurement of chemical composition, (e.g. the amount of water, fat etc. (ElMasry and Wold, 2008)), measurement of microbial spoilage (Huang et al., 2013; Wu and Sun, 2013), and detection of product defects (e.g. apple rot, parasites in fish etc. (Elmasry et al., 2012; Sivertsen et al., 2012)). HSI has also been applied for estimation of fish fillet shelf life and differentiation between fresh and frozen-thawed fillets (Sivertsen et al., 2011; Zhu et al., 2013).

For the fish industry, one of the most important quality parameters is the amount and distribution of blood in the fillet. Blood in the fish muscle is primarily caused by stress and bruising during catch, and/or inadequate bleeding of the fish after catch (Rotabakk et al., 2011). Blood in the fillet produces red stains and a general reddish discoloration that renders the product less appetizing.

Blood also acts as a catalyst for lipid oxidation during storage, causing a rancid smell and taste (Larsson et al., 2007; Richards and Hultin, 2002).

Absorption spectra for cod hemoglobin within the visible (VIS) part of the electromagnetic spectrum are shown in Figure 1 (Olsen and Elvevoll, 2011). The absorption spectrum varies with the oxidative state of the blood. When the fish is alive, the blood contains a mix of oxy- and deoxyhemoglobin, and after the fish is slaughtered and filleted, the hemoglobin gradually undergoes autoxidation and becomes methemoglobin. The absorption spectra for these hemoglobin states can be used to estimate blood concentration in hyperspectral images of fish fillets.

A heuristic approach to detect and visualize the presence of blood in the images is to study the hyperspectral image at a wavelength where light absorption by hemoglobin is relatively high for all oxidation states, for example 525 nm. To correct for variations in illumination and scattering, the image can be normalized using an image from a wavelength where absorption of hemoglobin is low, for example 715 nm. This approach has been used to detect the center line of the fillet, where the blood concentration is relatively high (Sivertsen et al., 2009). However, there are other effects that can yield a similar ratio of absorption between the two wavelengths, and the method is therefore not very robust. The method also does not utilize the full extent of information in the hyperspectral image.

In most applications of hyperspectral imaging, multivariate techniques are used to analyze the spectra. Several different applications have led to development of a large set of statistical analysis techniques, and the choice of technique for a specific problem is based on the nature of the data available. For example, if the spectroscopic measurement can be related to one or several known response variables (e.g. chemical concentrations), Partial Least Squares (PLS) models can be trained using the known responses, and then used to estimate unknown responses directly from spectral information (ElMasry et al., 2007; Wold et al., 2001). However, PLS modelling often represents a "black box" where the responses are estimated without the analyst really knowing what the regression coefficients mean. In this work, we employ a method termed *non-negativity constrained spectral unmixing,* which decomposes the measured spectrum into a set of absorption spectra known a priori. This physics-based approach yields results that are more easily interpreted than those of PLS or similar models. The technique is best known from remote sensing, where it is used to separate contributions from different types of rock, soil and vegetation with known reflection spectra (Keshava, 2003; van der Meer et al., 2012). Since the absorption spectra of hemoglobin are well known, the technique also has potential for detection of blood in fish fillets. To the best of our knowledge, this combination of hyperspectral imaging and spectral unmixing to estimate of blood in fish fillets is novel.
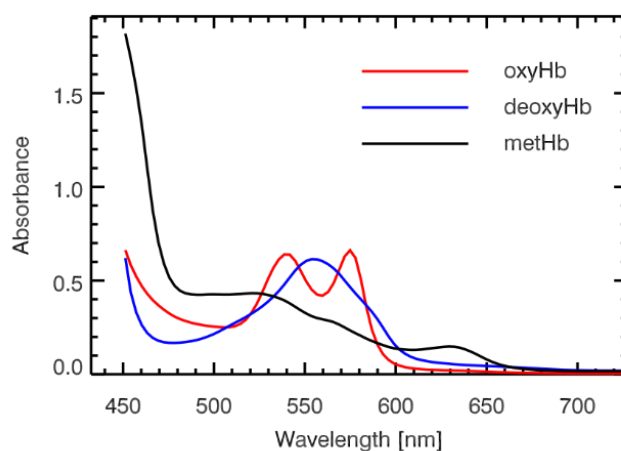

Figure 1: Absorption spectra for oxy-, deoxy- and methemoglobin measured by a spectrophotometer, with equal molar concentrations and equal path length (Olsen and Elvevoll, 2011).

The constrained spectral unmixing method is also combined with an estimation of effects caused by light scattering. Scattering in biological tissues is an active research field in itself, especially within the field of medicine, and a large set of scattering models and measurement methods have been developed (Cheong et al., 1990; Jacques, 2013; Jacques and Pogue, 2008). In general, the interaction between tissue and light is a complex function of the absorbance of different chromophores (e.g. blood) and the tissue scattering properties, and it is difficult to separate the two exactly in measurements. Wavelength-dependent scattering effects also introduce a wavelength-dependent optical path length in tissue, and modifications to the Beer-Lambert law have been proposed to include scattering and variable path length (Delpy et al., 1988; Sassaroli and Fantini, 2004).

In this work, we make the heuristic and simplifying assumption that the variable path length effect is negligible, and that the effect of scattering is to introduce a baseline shift in the measured absorbance spectra. The baseline is assumed to be a slowly varying function of wavelength and is modelled as a low-order polynomial. This approach is similar to the extended multiplicative scatter correction (EMSC) often applied in infrared spectroscopy (Afseth and Kohler, 2012; Martens et al., 2003). The same approach has also been applied for analysis of blood oxygenation in hyperspectral images, with good results (Gillies et al., 2003; Häggblad et al., 2010). In this work, we show that even though the scattering model is simple, it generally produces a good fit between with the measured and modelled spectra.

2 THEORY

2.1 ADDITIVE MIXING MODEL

The underlying assumption of the spectral unmixing model used here is that the total chemical absorption of light is a sum of absorption spectra for the different constituents in the mixture, weighted by their concentrations. In mathematical terms,

$$s_{ch,tot}(\lambda) = \sum_{i=1}^{N} a_i\, e_i(\lambda)\,, \tag{1}$$

where λ denotes wavelength, $s_{ch,tot}(\lambda)$ is the total chemical absorption spectrum, a_i and $e_i(\lambda)$ are the concentrations and absorption spectra of each chemical component, respectively, and N is the number of components. Note that path length for the light is assumed to be equal for each component. The concentrations a_i and absorption spectra $e_i(\lambda)$ are also referred to in the literature as *abundances* and *endmembers*, respectively (Keshava, 2003).

In practical measurements, the chemical absorption spectra are mixed together with effects of scattering. If these effects are modelled as a polynomial, as described in the introduction, the total measured spectrum $s_{meas}(\lambda)$ can be written as

$$s_{meas}(\lambda) = \sum_{i=1}^{N} a_i\, e_i(\lambda) + \sum_{i=1}^{M} b_i \lambda^{i-1}\,, \tag{2}$$

where the last sum corresponds to polynomials of the wavelength λ, of degree $M-1$. To simplify the notation and adapt it for linear algebra, Eq. (2) can be written as

$$\boldsymbol{s} = \boldsymbol{E}\boldsymbol{a} + \boldsymbol{\Lambda}\boldsymbol{b}\,, \tag{3}$$

where $s = [s_1, s_2, …, s_K]^T$ is the measured spectrum, sampled at K discrete wavelengths $[\lambda_1, \lambda_2, …, \lambda_K]$. The end member spectra are grouped together in $E = [e_1, e_2, …, e_N]$, where the individual spectra are given by $e_i = [e_{i,1}, e_{i,2}, …, e_{i,K}]^T$, and the end member abundances are contained in $a = [a_1, a_2, …, a_N]^T$. The term Λb is structured similarly to Ea, with the polynomial contained in the matrix $\Lambda = [\lambda^0, \lambda^1, …, \lambda^{M-1}]$, where $\lambda^i = [\lambda_1^i, \lambda_2^i …, \lambda_K^i]^T$, and the scattering coefficients are contained in $b = [b_1, b_2, …, b_M]^T$.

2.2 SPECTRAL UNMIXING

Spectral unmixing of the measured spectrum s is performed to estimate the individual abundances a_i, while simultaneously taking into account the effects of scattering. By their physical nature, the abundances cannot have a negative value, so $a_i \geq 0$, for all i. The scattering coefficients b_i are however not constrained in any way. Thus, Eq. (3) poses a mixed constraint problem. The problem can be separated into purely constrained and unconstrained parts, an approach known as separable least squares (Golub and Pereyra, 1973), by some algebraic manipulation. Equation (3) is rearranged into

$$\Lambda b = s - Ea . \tag{4}$$

A best-fit estimate for b is obtained from the normal linear least squares solution, yielding

$$\widehat{b} = \underbrace{(\Lambda^T \Lambda)^{-1} \Lambda^T}_{\Lambda^+} (s - Ea) , \tag{5}$$

where $\Lambda^+ = (\Lambda^T \Lambda)^{-1} \Lambda^T$ is the so-called pseudoinverse. The estimate $\widehat{b}$ is inserted for b in Eq. (3), yielding

$$\underbrace{(I - \Lambda \Lambda^+)}_{P} s = \underbrace{(I - \Lambda \Lambda^+)}_{P} Ea . \tag{6}$$

The "projection matrix" $P = I - \Lambda \Lambda^+$ is applied to both the measured spectrum s and to the end member spectra E, yielding modified spectra $Ps = \tilde{s}$ and $PE = \widetilde{E}$. The projection matrix transforms the spectra to a vector subspace where the least-squares solutions for the scattering coefficients b are already applied. The result is a purely constrained problem,

$$\tilde{s} = \widetilde{E}a, \quad a \geq 0 , \tag{7}$$

which can be solved with an algorithm adapted for non-negativity-constrained least squares (NNLS) problems. The de facto standard algorithm for NNLS was first introduced by Lawson and Hanson (Lawson and Hanson, 1974), and this is also the algorithm implemented in this work. A fast version of the algorithm is described in (Bro and De Jong, 1997). Solving Eq. (7) yields a least-squares solution $\widehat{a}$, which is inserted into Eq. (5) to obtain the scattering coefficients $\widehat{b}$.

3 MATERIALS AND METHODS

3.1 ENDMEMBER SPECTRA

Endmember spectra for hemoglobin in three different oxidation states (oxy-, deoxy- and methemoglobin) were taken from (Olsen and Elvevoll, 2011). Tabulated values for the spectra were obtained through personal communication with Stein H. Olsen. The three spectra were measured using a spectrophotometer, using the same path length and hemoglobin concentration in each measurement.

Tabulated values for the water absorption spectrum were taken from the high-resolution measurement described in (Pope and Fry, 1997). Since these values only cover the wavelength range

between 380-700 nm, the water spectrum was completed with tabulated values from (Hale and Querry, 1973), to cover wavelengths between 700 and 950 nm.

The five endmember spectra used in the model are shown in Figure 2 a). These also include a cod muscle spectrum, which was included to account for spectral effects which could not be explained by scattering, hemoglobin or water spectra. The muscle endmember spectrum was based on a hyperspectral image of a cod fillet with relatively little blood, determined through visual inspection of fillet color. However, all samples of cod muscle contain some amount of blood, in addition to a significant amount of water. The measurement is also affected by scattering effects. The cod spectrum was therefore pre-processed by applying the spectral unmixing model with blood, water and scattering as endmembers, and removing the contributions of these endmembers from the spectrum. Scattering was modelled as a polynomial of degree 1 (M = 2). This choice is explained in Section 3.2. The resulting corrected muscle spectrum is shown in Figure 2 b).

Note that the endmember spectra in Figure 2 a) have been normalized to have an equal area under the curve to easily compare the features of the spectra in the same plot. Also, since the spectra were measured at different experimental conditions, they are not directly comparable in terms of absolute absorbance. However, in this work it is the spectral shapes rather than the absolute values that are important for the method to work. In the spectral unmixing procedure, non-normalized spectra were used, and since the hemoglobin spectra were measured under the same conditions, the estimated abundances for the three hemoglobin states are directly comparable.

3.2 CHOICE OF SCATTERING PARAMETERS

The effect of scattering on the measured absorbance spectrum was modelled as a low-order polynomial, as described in the introduction and Section 2.1. During development of the methodology, polynomials of different degrees were tested. To ensure that the effect of scattering was smoothly varying across the spectral range, the polynomial degree was restricted to 2 or lower (M = 1, 2, or 3). Different values for M resulted in some differences in summed hemoglobin abundance for a set of test images. There were also differences in the relative abundances of oxy-, deoxy- and met-hemoglobin, but without any clear indication of which estimate was more plausible. The coefficient of determination, R^2 (Walpole et al., 2002), was used to assess the fit between the modelled spectra and measurements, and the fit generally increased with increasing M. This is expected, as an increase in polynomial order translates into more degrees of freedom for fitting the scattering contribution to the measured spectrum. However, use of a 2nd order polynomial seemingly lead to "overfitting" to the measured spectra, with a very large part of the absorption spectrum in the 430-650 nm range being explained as scattering. To avoid overfitting while still achieving a relatively high goodness of fit, the scattering polynomial order was set to 1 (M = 2) for all results presented in this work.

3.3 HYPERSPECTRAL IMAGING

Hyperspectral images were recorded using a VNIR-640 imaging spectrograph (Norsk Elektro Optikk, Skedsmokorset, Norway), which operates in a pushbroom imaging mode. The spectrograph was fitted with a lens focused at 1 meter distance with a 50 mm depth of field. The spatial resolution was 0.5 x 0.5 mm, and the spectral resolution was 10 nm for the spectral range of 430-1000 nm.

The spectrograph was mounted 1020 mm above a conveyor belt carrying the samples to be imaged. The samples were illuminated with a custom-made light source, which consists of 14 halogen bulbs (50 W) mounted inside a box consisting of 10 mm thick high-density polytetrafluoroethylene (PTFE, also known as Teflon) plates. The box was designed to make the light from the bulbs reflect from the walls before exiting onto the conveyor belt, to create a uniform and diffuse illumination, as shown in Figure 3. To minimize the effect of ambient light, all other lights were turned off during measurements.
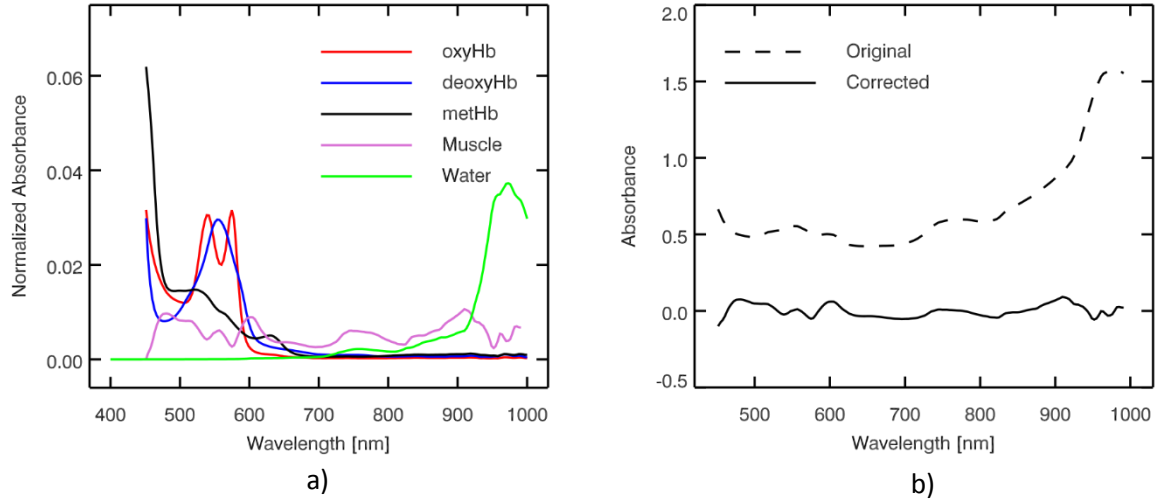
Figure 2: Endmember spectra included in the analysis. a) Absorption spectra of water, muscle and blood in different oxidation states, normalized for equal area under the curve. b) Cod muscle absorption spectrum, before and after unmixing and removal contributions from blood, water and scattering.

All processing of hyperspectral data was performed using IDL (Exelis Visual Information Solutions, Bracknell, United Kingdom).

The raw image recorded by the camera includes effects due to spatial variation in illumination and the spectral characteristics of the halogen lamps. To correct for these and convert the image into absolute reflectance values, a calibration standard was imaged before each hyperspectral measurement series. The standard consisted of a large high-density PTFE plate with a smaller inset plate made of optical grade low-density PTFE (Spectralon, manufactured by LabSphere, Inc., North Sutton, New Hampshire, USA). The low-density PTFE has over 99% diffuse reflectance in the 430-1000 nm range of the camera, while high-density PTFE has a diffuse reflectance of approximately 95 % around 430 nm, which drops to approximately 80 % at 1000 nm (Tsai et al., 2008).

The spatial variation of the illumination was measured by extracting an image line from the high-density PTFE plate, $I_{\text{HD-PTFE}}(\lambda, x)$. The lamp characteristics were measured by extracting the spectrum from a single pixel from the low-density PTFE plate, $I_{\text{LD-PTFE}}(\lambda, x_k)$, where x_k denotes the spatial coordinate of the pixel. These measurements were used to calibrate each subsequent image,

$$
S_{\text{meas}}(\lambda, x, y) = -\ln\left(\underbrace{\left(\frac{I_{\text{meas}}(\lambda, x, y)}{I_{\text{HD-PTFE}}(\lambda, x)} \right)}_{\text{Spatial corr.}} \cdot \underbrace{\left(\frac{I_{\text{HD-PTFE}}(\lambda, x_k)}{I_{\text{LD-PTFE}}(\lambda, x_k)} \cdot 0.99 \right)}_{\text{Spectral corr.}} \right) , \tag{8}
$$

where $I_{\text{meas}}(\lambda, x, y)$ is the uncalibrated image, and the logarithm is used to convert the image units from light reflectivity to apparent absorbance. The factor 0.99 is used to account for the 99% diffuse reflectance of the low-density PTFE.

Color images were synthesized from the hyperspectral images using a CIE 1964 10 degree standard observer model and a CIE D65 daylight illumination model (Wyszecki and Stiles, 1982).

3.4 Reference measurements on homogenized cod muscle

Reference samples with known concentrations of blood were made by homogenizing cod muscle and adding different quantities of blood. Blood was acquired from Atlantic cod kept at the Tromsø Aquaculture Research Station in Tromsø, Norway. The cod was carefully netted from a cage and killed immediately with a blow to the head. Blood was collected from the caudal vein and stored

at 4°C in 4 ml tubes spray coated with Lithium Heparin to avoid coagulation. Samples of homogenized cod muscle were made from fillets purchased at a local supermarket. According to the staff, the cod had arrived three days before purchase. The fillets were trimmed to remove skin, dark muscle, and small blood spots and homogenized by running them twice though a meat grinder. The homogenized muscle was thoroughly mixed by hand to ensure a uniform distribution of the blood already present in the muscle.

The blood was lysed by adding 2% of Triton X-100 (Sigma-Aldrich, St. Louis, Missouri, USA), to break up the membranes of the blood cells and make the hemoglobin easier to mix with the muscle. The lysate was then diluted with deionized water to obtain relative blood concentrations in the range 2.5-100 %. 3 ml of each blood-water mixture was added to 150 g of homogenized muscle, mixed by hand for approximately 2 minutes and put into rectangular plastic Petri dishes (100 x 100 x 15 mm). A control sample with 150 g muscle and no added blood was also included. The samples were placed together on a plate and imaged with the hyperspectral imaging setup described in section 3.2.

A modified Hornsey hematin method (Hornsey, 1956) was used to determine the concentration of total heme pigment in the homogenized muscle and the blood lysate. The method converts all forms of hemoglobin into acid hematin, and thus measures only the total hemoglobin concentration, not the individual concentrations of oxy-, deoxy- and methemoglobin.

Three 5 g replicates of minced muscle and three 0.5 ml replicates of blood lysate were used. The samples were placed in 50 ml centrifuge tubes and diluted with de-ionized water (0.5 ml for muscle samples, 4 ml for lysate). 20 ml of acetone and 0.5 ml of 37% hydrochloric acid (HCl) were added to each sample, and the mixture was vortexed for 15 s and then stored in a refrigerator at 4 °C. After 60 min, the mixture was filtered through a Whatman no. 1 filter paper. The filtrate was centrifuged at 10 000 G for 15 min, before measuring the absorbance at 512 nm using a UV-1800 UV-VIS spectrophotometer (Shimadzu Europe GmbH, Germany). The amount of heme pigment was calculated using a standard curve made from bovine hemoglobin (Sigma-Aldrich, St. Louis, Missouri, USA).
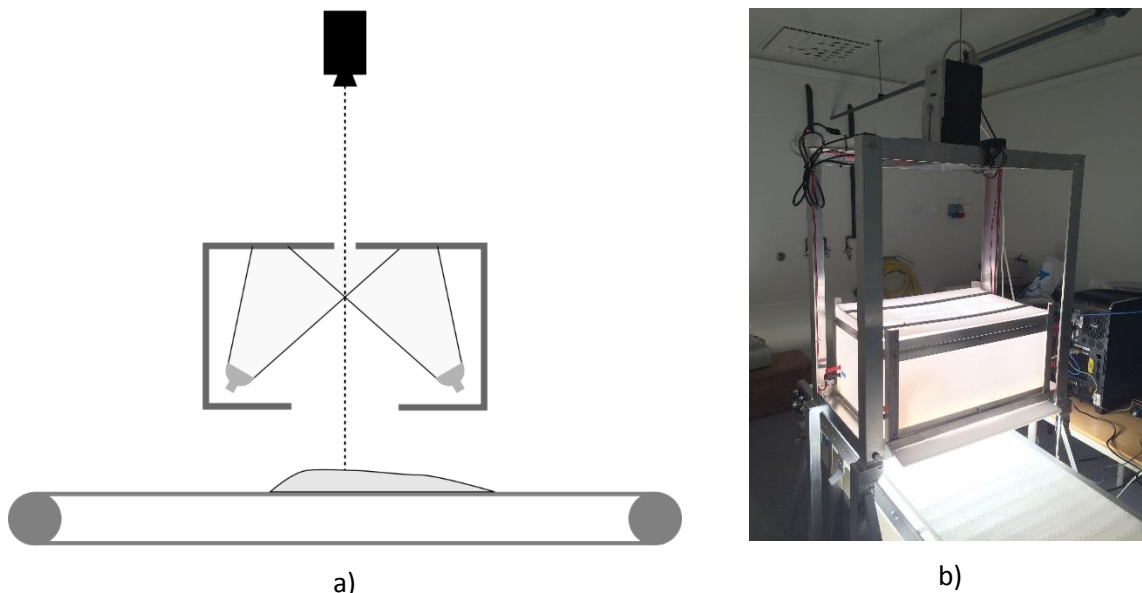

a)

b)

Figure 3: Hyperspectral imaging setup with custom made illumination box. a) Schematic drawing showing a side view of the conveyor belt. The camera line of view is indicated with a dashed line. b) Picture of the imaging setup.:

3.5 FISH FILLET SAMPLES WITH VARYING AMOUNTS OF BLOOD

Atlantic cod (n=9) were selected by researchers from Nofima AS at a fish landing facility at Husøy (Senja, Norway), on February 9. 2017. The landed fish were collected from vessels using either gill nets or seines. The fish were selected based on exterior appearance to represent a spectrum from good to bad quality with regard to blood.

The fish was packed in polystyrene boxes and transported on ice to the Nofima facilities and were filleted and imaged using the hyperspectral imaging setup on Feb. 10. Out of 18 fillets, 4 fillets with varying amounts of blood were selected to demonstrate the method described in this paper.

4 RESULTS

4.1 DEMONSTRATION OF UNMIXING FOR SINGLE SPECTRUM

Figure 4 demonstrates the removal of scattering effects and the spectral unmixing for a spectrum taken from a single pixel of a hyperspectral image of a cod fillet. In Figure 4 a), the original spectrum is shown as a continuous line, and the effect of scattering is modelled as a 1st-degree polynomial, shown as a dashed line. The scatter corrected spectrum (the original spectrum with the scatter polynomial subtracted) is shown as a dash-dot line.

In Figure 4 b), the scatter corrected spectrum is shown as a black continuous line. The unmixed spectra of muscle, water and hemoglobin in different states is shown as green, blue and red lines, respectively. The sum of the unmixed spectra, which represents the best-fit model of the measured spectrum, is plotted as a black dashed line. The modelled spectrum follows the measured spectrum closely, indicating that the fit is relatively good.

4.2 RESULTS FOR HOMOGENIZED SAMPLES

A color image of the homogenized samples with controlled concentrations of added blood is shown in Figure 5, together with example spectra from some of the samples. The main difference between the spectra is the amount of absorption in the range 450-650 nm, which is explained by the difference in hemoglobin concentration. The estimated scattering effects, indicated as dashed blue lines, change slightly with blood concentration; at low concentrations, the loss of light due to scattering is highest at long wavelengths, while at high concentrations, the loss of light is highest at short wavelengths. The scattering properties of the muscle itself should be the same for all samples, and the observed effect indicates that the spectral unmixing model (and its underlying assumptions) cannot completely separate absorption and scattering. However, the fit between the measured spectra and the spectra modelled by unmixing, as indicated by R^2, is quite good both for low and high hemoglobin concentrations. This shows that the unmixing model is able to account for the spectral variations in the data.

Figure 6 shows the abundancies for each endmember as a function of hemoglobin concentration in the homogenized samples. The abundancies are mean values based on image regions covering the center of each sample, covering approximately 18000 measurement pixels (corresponding to 45 cm^2) per sample. The methemoglobin abundancy is relatively constant for all the samples, which is expected, since the artificially added blood contains mostly oxy- and deoxyhemoglobin. The abundancies for oxy- and deoxyhemoglobin increase monotonically with hemoglobin concentration, but the curves flatten at higher concentrations, indicating a non-linear relationship between abundancies and concentration.

The muscle and water abundancies increase slightly with increasing hemoglobin concentration, even though the samples are identical except for varying amounts of hemoglobin. This indicates that the unmixing method cannot completely de-couple the effects of the different abundancies and that some of the variation in hemoglobin is translated into variation in muscle and water abundancies. Note however, that the relative change is much smaller than compared to the change for oxy- and deoxyhemoglobin.

The three abundancies for blood can be summed into a total blood abundance. Figure 7 shows the relationship between the mean total blood abundance and hemoglobin concentration for each sample and an exponential model fitted to the curve. The exponential model is of the form:

$$c = A\big(\exp\big(B \cdot a_{\text{blood,total}}\big) - 1\big) \ , \tag{9}$$

where c is the hemoglobin concentration in mg per g muscle, $a_{\text{blood,total}}$ is the sum of the three blood abundancies, and A and B are constants which are calculated to fit the curve. The exponential model can be used to translate any total blood abundance value (within the data range used to fit the model) to a hemoglobin concentration value. This is demonstrated in Figure 8, which shows both an image of total blood abundance for the homogenized samples, and a corresponding image of hemoglobin concentration, calculated using the exponential model. Note that the conversion both represents a correction of the baseline level (samples with low concentrations appear lighter) and a correction for non-linearity between total blood abundance and hemoglobin concentration. The samples with the highest concentrations show some heterogeneity, which could be due to heterogeneous properties of the muscle and/or imperfect mixing of muscle and blood.
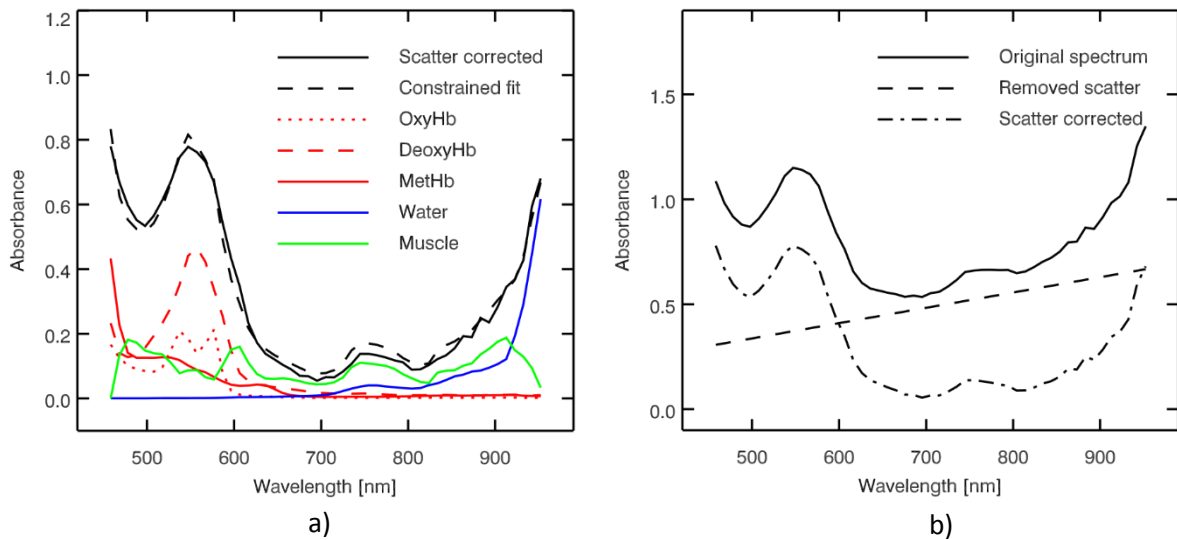

Figure 4: Demonstration of spectral unmixing for a single pixel spectrum. a) Originally measured spectrum, scattering effects estimated as 1st-degree polynomial, and spectrum with scattering effects subtracted. b) Measured spectrum (scatter corrected) with spectrum modelled as a sum of blood, water and muscle endmembers.
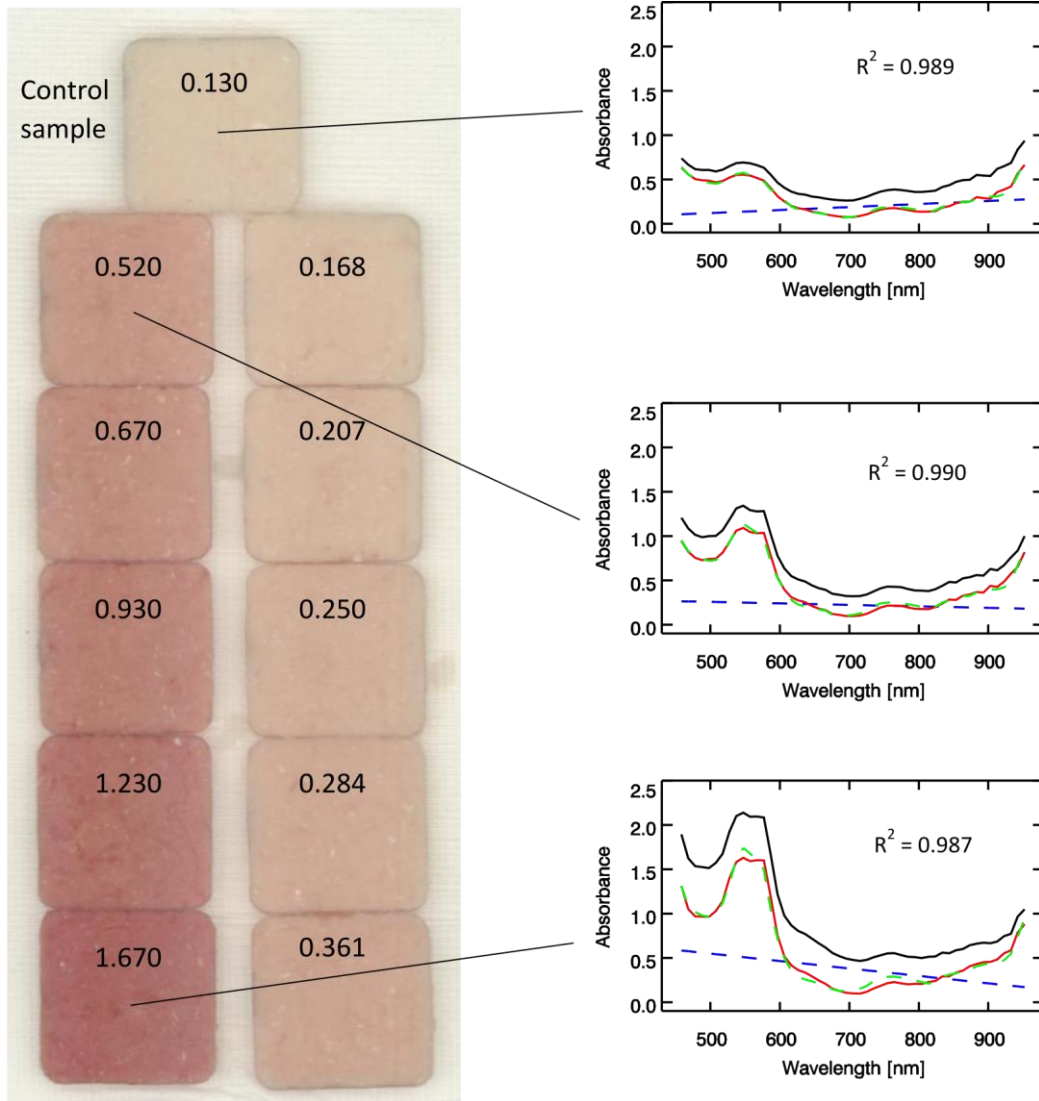
Figure 5: Color image of homogenized cod muscle with different amounts of artificially added blood. The chemically measured hemoglobin concentration in mg per g muscle is indicated for each sample. Example spectra from some of the samples are also shown, with black lines indicating the original spectrum, dashed blue lines indicating estimated scattering effects, red lines indicating the scatter corrected spectrum and dashed green lines indicating fitted spectrum from the unmixing model. The fit between the measured and the modelled spectrum is indicated with R2 correlation coefficients.:
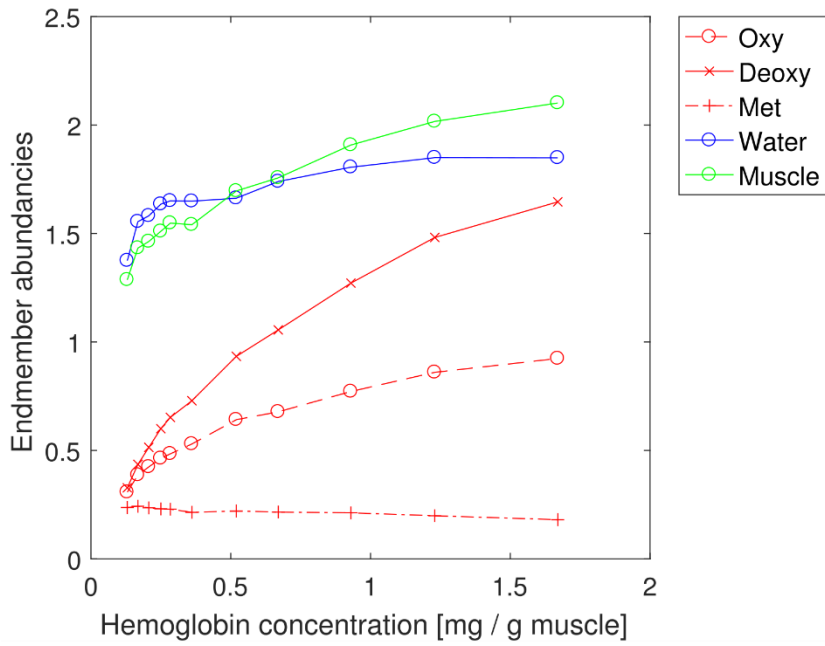
Figure 6: Endmember abundancies as function of hemoglobin concentration in homogenized samples (average values from center area of each sample).
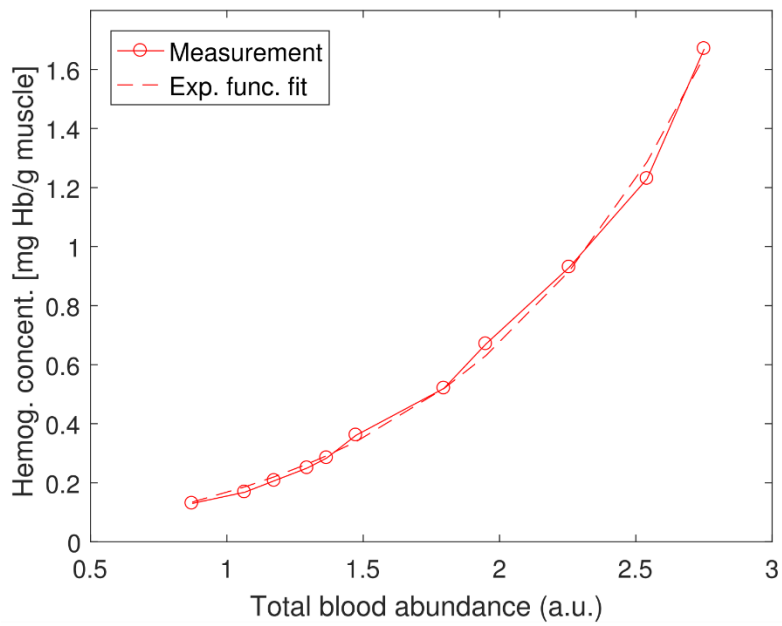

Figure 7: Polynomial model of hemoglobin concentration in muscle as a function of total blood abundance (sum of oxy-, deoxy- and methemoglobin abundancies).
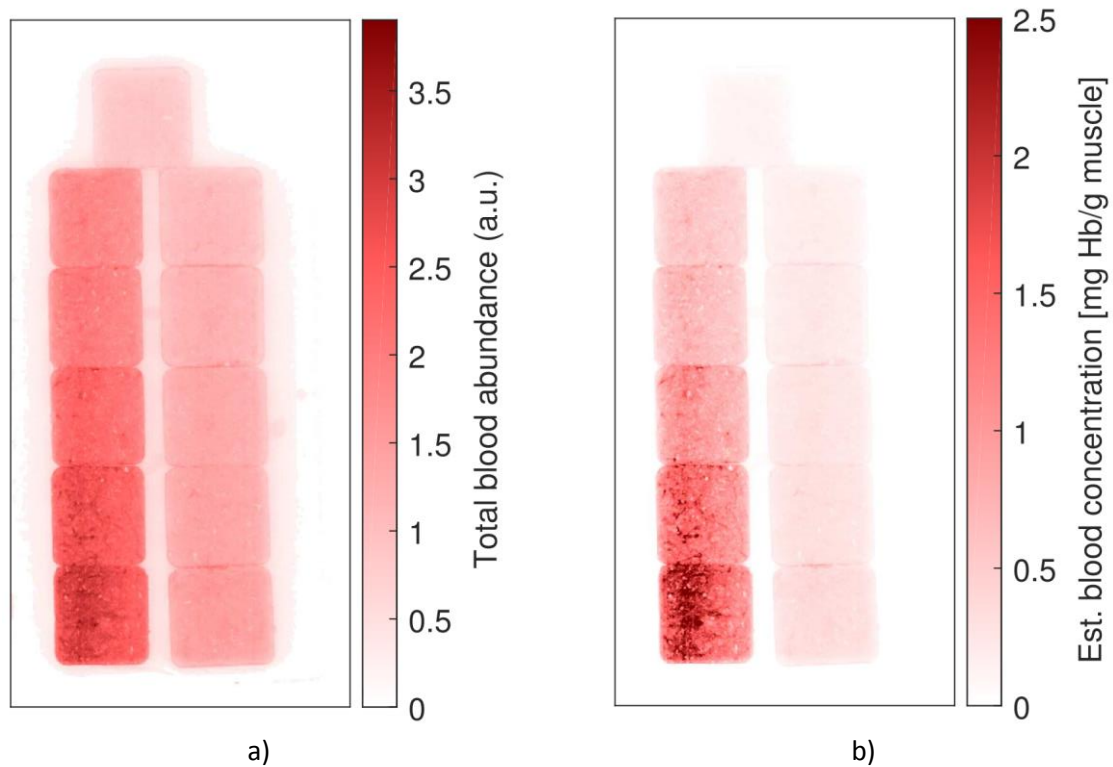
Figure 8: Conversion of blood abundance to hemoglobin concentration, demonstrated on image of homogenized samples. a) Total blood abundance. b) Hemoglobin concentration, calculated using exponential model shown in Figure 7.

4.3 BLOOD ANALYSIS FOR FILLETS WITH DIFFERENT AMOUNTS OF BLOOD

To demonstrate the performance of the spectral unmixing method, hyperspectral images of four different fillets were analyzed, and hemoglobin concentration was calculated using the exponential model. Color images and blood concentration images are shown in Figure 9. The fillets are sorted according to increasing blood concentration and number of blood defects.

All the blood analysis images show a line running along the middle of the fillet with small spots of increased blood levels. The line corresponds to blood vessels along the backbone of the fish that were cut during filleting. The fillet shown in a) and e), which is an example of a high-quality fillet, generally has a low amount of blood in the muscle and only a small blood spot in the very top, toward the neck. The fillet shown in b) and f) also has low blood levels, but has a small blood spot close to the center of the fillet, which could be considered a defect in some cases. The fillet in c) and g) has a slightly elevated amount of blood in the muscle and also has several large blood spots along the center line. These defects are serious and will, in most cases, cause the fillet to be down-graded (not top quality). The last fillet, shown in d) and h), has very elevated blood levels throughout the muscle and also several blood spots, making it a decidedly low-quality fillet.
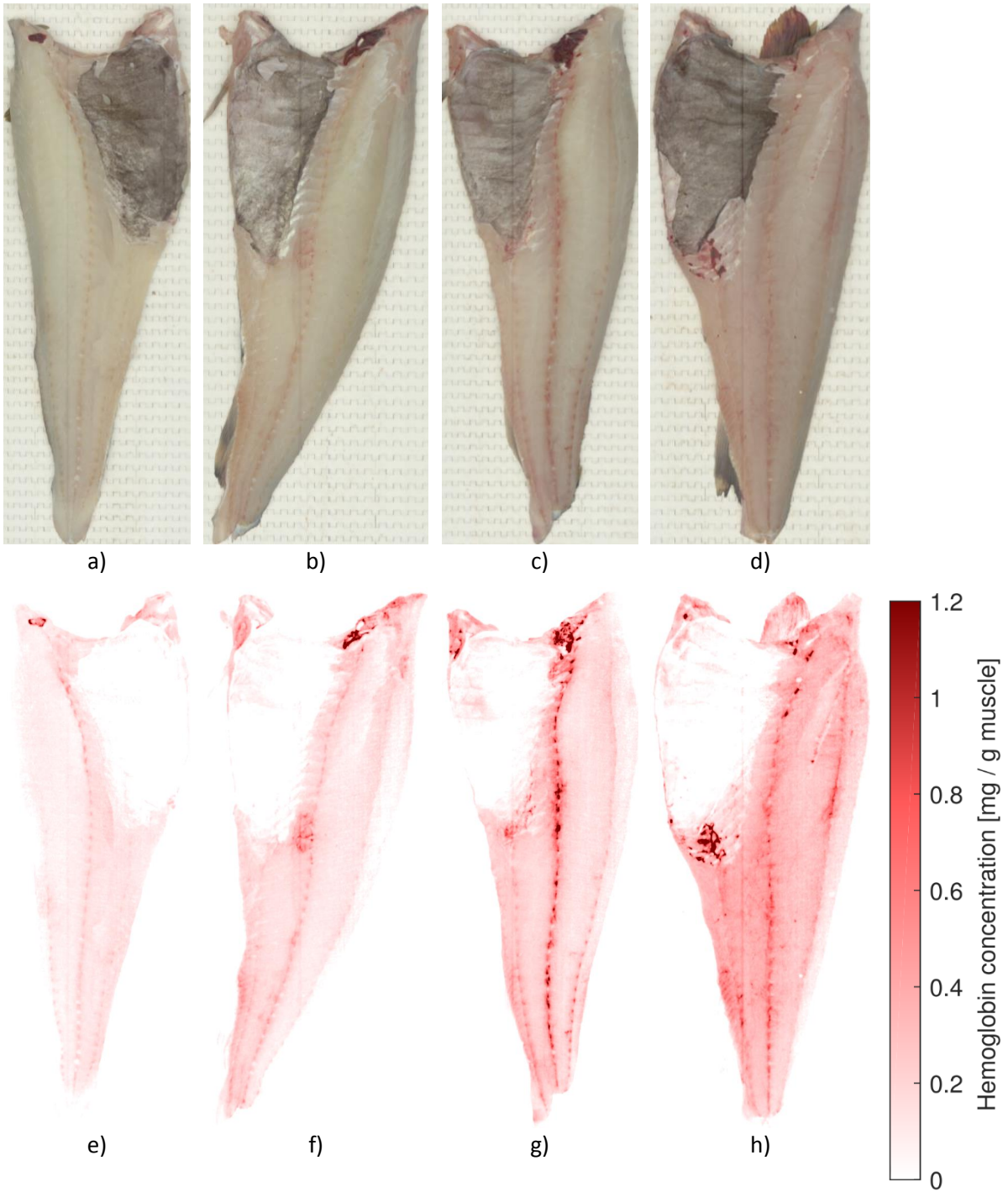
Figure 9: Color images (a-d) and corresponding blood concentration images (e-h) from four example fillets. The black lining in the belly was not removed prior to imaging, resulting in the white areas in the blood analysis images. The vertical stripe seen in some of the images is due to a few weak pixels in the hyperspectral camera.

5 DISCUSSION

We have described and demonstrated a spectral unmixing approach for analysis of blood in hyperspectral images of cod fillets. The method is based on a priori knowledge of the absorbance properties of blood in different oxidation states, in addition to absorption in water and muscle. The modelled spectra show a very good fit to the measured spectra for several cases with varying amounts of blood in the fillets. By using reference measurements with known concentrations of blood, it is also possible to make quantitative estimates of hemoglobin concentration based on the unmixing results. The method is general in nature and can be expanded to include additional constituents of fish fillets, such as fat, melanin etc.

The blood measurement method was demonstrated for cod fillets in this work, but we also expect the method to be applicable to other fish species. The performance for other white fish species should be comparable to that of cod, while species with reddish muscle color, such as salmon, may be more challenging due to the spectral overlap between hemoglobin and muscle pigments (Ottestad et al., 2011). The method may also be applicable for detection of blood in other types of meat, for example in chicken meat, where blood spots and heightened blood levels are regarded as a major quality defect (Alvarado et al., 2007).

The reference measurements for hemoglobin concentration were performed on homogenized samples of cod muscle. This ensures that, unlike samples taken from intact cod fillets, the samples have a relatively uniform distribution of blood. However, homogenizing the muscle also changes its light scattering properties by cutting long muscle fibers into smaller parts and creating small air pockets in the sample. The practical effect of this difference between reference samples and intact fillets has so far not been studied but will be the subject of a future study. The differences in scattering properties should be accounted for to some degree by the estimation of scattering effects in the spectral unmixing method. The blood concentration images shown in Figure 7 also appear slightly speckled, especially at high blood concentrations. This is probably due to the heterogeneous nature of the minced muscle samples, with bright spots being caused by pieces of connective tissue, and dark spots being caused by slightly non-uniform distribution of blood. However, the exponential model used for estimation of hemoglobin concentration is based on mean values from a large area from each sample, and we therefore believe that the estimation of hemoglobin concentration from hyperspectral images is relatively accurate.

By including spectra for oxy-, deoxy- and methemoglobin in the spectral unmixing model, we enable estimation of the abundance of each of these individual endmembers. During storage, oxy- and deoxyhemoglobin in blood oxidizes into the methemoglobin state, and the relative abundance of methemoglobin may therefore be useful for shelf life estimation (Sivertsen et al., 2011). Using all three endmembers also enables the estimation of total blood abundance independent of the oxidation process. However, the reference method used to measure hemoglobin concentration in the homogenized samples only measures total hemoglobin, and is not able to distinguish between the three states. The results shown in Figure 6 indicate that the amount of methemoglobin is low and relatively constant for all the homogenized samples. In future work, reference measurements could be expanded to include samples where methemoglobin concentrations are expected to be higher, for example frozen-thawed samples. Oxy- and deoxyhemoglobin could also be chemically converted to methemoglobin prior to being mixed into a homogenized sample by adding potassium ferricyanide ($K_3Fe(CN)_6$) (Olsen and Elvevoll, 2011).

The relationship between blood concentration and blood abundancies is non-linear, as shown in Figure 6. At high concentrations, the curve "flattens out". A possible explanation for this is that the average path length of the light inside the sample changes as function of hemoglobin concentration. When the concentration is low, absorption of light inside the sample is also low, and the light which is emitted from the sample surface is a result of backscattered light both from the surface and from

deeper within the sample. When the concentration is high, the light that travels far into the sample is absorbed before it can be backscattered towards the surface, and the emitted light from the sample surface consists of light that has travelled a shorter average distance inside the sample. This absorption-dependent path length effect leads to a non-linear relationship between concentration and absorption, and thus also between concentration and abundancies.

The muscle endmember is based on a spectrum from a hyperspectral image of cod and corrected for the contributions from hemoglobin and water absorption using spectral unmixing. This is a heuristic approach which "fills the gap" between the set of independently measured endmembers and practical measurements of fillets, enabling spectral unmixing with a good model fit for most cases. A previous study found that for extractions of pure cod muscle in water and methanol, there is very little absorption in the 300-600 nm region (Stormo et al., 2004). This finding could indicate that the muscle endmember used in the current work partly describes inaccuracies between the model and the practical measurements, in addition to some absorbance due to compounds in the muscle. In future work, we aim to understand the absorbance in muscle better and, if possible, replace the muscle endmember with endmembers of known chemical compounds.

The peak at approximately 605 nm in the corrected muscle spectrum could possibly be attributed to cytochrome oxidase, the terminal enzyme in the respiratory chains of mitochondria. The enzyme contains the two cytochromes a and $a3$, which each contain haem A, and has absorption peaks at 445 and 605 nm (Mathews et al., 1999; Yonetani, 1960). Inclusion of cytochrome oxidase in models of light absorption in tissue has been shown to improve model fit in an application with fiber-optic reflectance imaging of heart tissue in calves (Lindbergh et al., 2010). If the observed peak in the corrected muscle spectrum is indeed due to cytochrome oxidase, inclusion of a cytochrome oxidase endmember could improve the model.

One of the main applications for the method described here is classification of fillets according to blood defects. Currently, such classification is often done manually and subjectively during fillet production. Training data for automatic classification could be established by using an expert panel to classify a large set of fillets according to perceived quality. The same fillets could then be imaged with a hyperspectral camera and analyzed using the method described here. This would allow thresholds for automatic quality grading to be set using quantitative thresholds on hemoglobin concentration. Separate thresholds could be set for different parts of the fillet (loin, belly, tail), which often are portioned into products of different value.

Hysperspectral cameras are generally far more expensive than standard cameras, making them less accessible as an option for industrial applications. However, the method described in this work can potentially be simplified by reducing the number of spectral bands, as demonstrated in (ElMasry et al., 2007). If a limited number of bands yield a sufficient accuracy, imaging can be performed by use of a standard monochrome camera combined with narrow bandpass filters, and/or by alternating between LED lights transmitting in key spectral bands.

6   CONCLUSIONS

We have described and demonstrated a spectral unmixing approach for detection of blood in diffuse reflectance hyperspectral images of cod fillets. The method is based on a priori knowledge of the absorbance properties of blood in different oxidation states, in addition to absorption in water and muscle. The method also includes estimation of scattering effects, which are modelled as a linear function of wavelength. The unmixing model generally yields a very good fit between measured and modelled spectra, and by using reference measurements with known blood concentrations, the model also enables quantitative estimation of blood concentration in the fillet surface. This high-resolution mapping of blood represents a useful tool for quality grading in the whitefish processing industry.

7 ACKNOWLEDGEMENTS

8 REFERENCES

Afseth, N.K., Kohler, A., 2012. Extended multiplicative signal correction in vibrational spectroscopy, a tutorial. Chemom. Intell. Lab. Syst. 117, 92–99. doi:10.1016/j.chemolab.2012.03.004

Alvarado, C.Z., Richards, M.P., O'Keefe, S.F., Wang, H., 2007. The Effect of Blood Removal on Oxidation and Shelf Life of Broiler Breast Meat. Poult. Sci. 86, 156–161. doi:10.1093/ps/86.1.156

Bro, R., De Jong, S., 1997. A Fast Non-Negativity-Constrained Least Squares Algorithm. J. Chemom. 11, 393–401.

Cheong, W.F., Prahl, S.A., Welch, A.J., 1990. A review of the optical properties of biological tissues. IEEE J. Quantum Electron. 26, 2166–2185. doi:10.1109/3.64354

Delpy, D.T., Cope, M., Zee, P. van der, Arridge, S., Wray, S., Wyatt, J., 1988. Estimation of optical pathlength through tissue from direct time of flight measurement. Phys. Med. Biol. 33, 1433–1442. doi:10.1088/0031-9155/33/12/008

Elmasry, G., Kamruzzaman, M., Sun, D.-W., Allen, P., 2012. Principles and applications of hyperspectral imaging in quality evaluation of agro-food products: a review. Crit. Rev. Food Sci. Nutr. 52, 999–1023. doi:10.1080/10408398.2010.543495

ElMasry, G., Wang, N., ElSayed, A., Ngadi, M., 2007. Hyperspectral imaging for nondestructive determination of some quality attributes for strawberry. J. Food Eng. 81, 98–107. doi:10.1016/j.jfoodeng.2006.10.016

ElMasry, G., Wold, J.P., 2008. High-speed assessment of fat and water content distribution in fish fillets using online imaging spectroscopy. J. Agric. Food Chem. 56, 7672–7. doi:10.1021/jf801074s

Gillies, R., Freeman, J.E., Cancio, L.C., Brand, D., Hopmeier, M., Mansfield, J.R., 2003. Systemic effects of shock and resuscitation monitored by visible hyperspectral imaging. Diabetes Technol. Ther. 5, 847–55. doi:10.1089/152091503322527058

Golub, G.H., Pereyra, V., 1973. The Differentiation of Pseudo-Inverses and Nonlinear Least Squares Problems Whose Variables Separate. SIAM J. Numer. Anal. 10, 413–432.

Gowen, A., O'Donnell, C., Cullen, P., Downey, G., Frias, J., 2007. Hyperspectral imaging – an emerging process analytical tool for food quality and safety control. Trends Food Sci. Technol. 18, 590–598. doi:10.1016/j.tifs.2007.06.001

Hale, G.M., Querry, M.R., 1973. Optical Constants of Water in the 200-nm to 200-microm Wavelength Region. Appl. Opt. 12, 555–63. doi:10.1364/AO.12.000555

Hornsey, H.C., 1956. The colour of cooked cured pork. I.—Estimation of the Nitric oxide-Haem Pigments. J. Sci. Food Agric. 7, 534–540. doi:10.1002/jsfa.2740070804

Huang, L., Zhao, J., Chen, Q., Zhang, Y., 2013. Rapid detection of total viable count (TVC) in pork meat by hyperspectral imaging. Food Res. Int. 54, 821–828. doi:10.1016/j.foodres.2013.08.011

Häggblad, E., Petersson, H., Ilias, M.A., Anderson, C.D., Salerud, E.G., 2010. A diffuse reflectance spectroscopic study of UV-induced erythematous reaction across well-defined borders in human skin. Skin Res. Technol. 16, 283–90. doi:10.1111/j.1600-0846.2010.00424.x

Jacques, S.L., 2013. Optical properties of biological tissues: a review. Phys. Med. Biol. 58, R37-61.

doi:10.1088/0031-9155/58/11/R37

Jacques, S.L., Pogue, B.W., 2008. Tutorial on diffuse light transport. J. Biomed. Opt. 13, 41302. doi:10.1117/1.2967535

Keshava, N., 2003. A survey of Spectral Unmixing Algorithms. Lincoln Lab. J. 14, 55–78.

Kruse, F.A., 1996. Identification and mapping of minerals in drill core using hyperspectral image analysis of infrared reflectance spectra. Int. J. Remote Sens. 17, 1623–1632. doi:10.1080/01431169608948728

Larsson, K., Almgren, A., Undeland, I., 2007. Hemoglobin-mediated lipid oxidation and compositional characteristics of washed fish mince model systems made from cod (Gadus morhua), herring (Clupea harengus), and salmon (Salmo salar) muscle. J. Agric. Food Chem. 55, 9027–35. doi:10.1021/jf070522z

Lawson, C.L., Hanson, R.J., 1974. Solving least squares problems. Prentice-Hall.

Lindbergh, T., Larsson, M., Szabó, Z., Casimir-Ahn, H., Strömberg, T., 2010. Intramyocardial oxygen transport by quantitative diffuse reflectance spectroscopy in calves. J. Biomed. Opt. 15, 27009. doi:10.1117/1.3374050

Lu, G., Fei, B., 2014. Medical hyperspectral imaging: a review. J. Biomed. Opt. 19, 10901. doi:10.1117/1.JBO.19.1.010901

Martens, H., Nielsen, J.P., Engelsen, S.B., 2003. Light Scattering and Light Absorbance Separated by Extended Multiplicative Signal Correction. Application to Near-Infrared Transmission Analysis of Powder Mixtures. Anal. Chem. 75, 394–404. doi:10.1021/ac020194w

Mathews, C.K., van Holde, K.E., Ahern, K.G., 1999. Biochemistry, 3rd ed. Pearson.

Olsen, S.H., Elvevoll, E.O., 2011. pH-induced shift in hemoglobin spectra: a spectrophotometeric comparison of atlantic cod (Gadus morhua) and mammalian hemoglobin. J. Agric. Food Chem. 59, 1415–22. doi:10.1021/jf1036273

Olsen, S.H., Sørensen, N.K., Larsen, R., Elvevoll, E.O., Nilsen, H., 2008. Impact of pre-slaughter stress on residual blood in fillet portions of farmed Atlantic cod (Gadus morhua) — Measured chemically and by Visible and Near-infrared spectroscopy. Aquaculture 284, 90–97. doi:10.1016/j.aquaculture.2008.07.042

Ottestad, S., Sørheim, O., Heia, K., Skaret, J., Wold, J.P., 2011. Effects of storage atmosphere and heme state on the color and visible reflectance spectra of salmon (Salmo salar) fillets. J. Agric. Food Chem. 59, 7825–31. doi:10.1021/jf201150x

Pope, R.M., Fry, E.S., 1997. Absorption spectrum (380–700 nm) of pure water II Integrating cavity measurements. Appl. Opt. 36, 8710. doi:10.1364/AO.36.008710

Richards, M.P., Hultin, H.O., 2002. Contributions of Blood and Blood Components to Lipid Oxidation in Fish Muscle. J. Agric. Food Chem. 50, 555–564. doi:10.1021/jf010562h

Rotabakk, B.T., Skipnes, D., Akse, L., Birkeland, S., 2011. Quality assessment of Atlantic cod (Gadus morhua) caught by longlining and trawling at the same time and location. Fish. Res. 112, 44–51. doi:10.1016/j.fishres.2011.08.009

Sassaroli, A., Fantini, S., 2004. Comment on the modified Beer-Lambert law for scattering media. Phys. Med. Biol. 49, N255–N257. doi:10.1088/0031-9155/49/14/N07

Sivertsen, A.H., Chu, C.-K., Wang, L.-C., Godtliebsen, F., Heia, K., Nilsen, H., 2009. Ridge detection with application to automatic fish fillet inspection. J. Food Eng. 90, 317–324. doi:10.1016/j.jfoodeng.2008.06.035

Sivertsen, A.H., Heia, K., Hindberg, K., Godtliebsen, F., 2012. Automatic nematode detection in cod fillets (Gadus morhua L.) by hyperspectral imaging. J. Food Eng. 111, 675–681.

Sivertsen, A.H., Kimiya, T., Heia, K., 2011. Automatic freshness assessment of cod (Gadus morhua) fillets by Vis/Nir spectroscopy. J. Food Eng. 103, 317–323. doi:10.1016/j.jfoodeng.2010.10.030

Stormo, S.K., Ernstsen, A., Nilsen, H., Heia, K., Sivertsen, A.H., Elvevoll, E., 2004. Compounds of parasitic roundworm absorbing in the visible region: target molecules for detection of roundworm in Atlantic cod. J. Food Prot. 67, 1522–5.

Thenkabail, P.S., Lyon, J.G., Huete, A. (Eds.), 2011. Hyperspectral Remote Sensing of Vegetation. CRC Press.

Tsai, B.K., Allen, D.W., Hanssen, L.M., Wilthan, B., Zeng, J., 2008. A comparison of optical properties between solid PTFE (Teflon) and (low density) sintered PTFE, in: Proc. SPIE 7065, Reflection, Scattering, and Diffraction from Surfaces, 70650Y (August 29, 2008). doi:10.1117/12.798138

van der Meer, F.D., van der Werff, H.M.A., van Ruitenbeek, F.J.A., Hecker, C.A., Bakker, W.H., Noomen, M.F., van der Meijde, M., Carranza, E.J.M., Smeth, J.B. de, Woldai, T., 2012. Multi- and hyperspectral geologic remote sensing: A review. Int. J. Appl. Earth Obs. Geoinf. 14, 112–128. doi:10.1016/j.jag.2011.08.002

Walpole, R.E., Myers, R.H., Myers, S.L., Ye, K., 2002. Probability and statistics for engineers and scientists, 7th ed. Prentice Hall.

Wold, S., Sjöström, M., Eriksson, L., 2001. PLS-regression: a basic tool of chemometrics. Chemom. Intell. Lab. Syst. 58, 109–130. doi:10.1016/S0169-7439(01)00155-1

Wu, D., Sun, D.-W., 2013. Potential of time series-hyperspectral imaging (TS-HSI) for non-invasive determination of microbial spoilage of salmon flesh. Talanta 111, 39–46. doi:10.1016/j.talanta.2013.03.041

Wyszecki, G., Stiles, W.S., 1982. Color Science, 2nd ed. Wiley.

Yonetani, T., 1960. Studies on Cytochrome Oxidase: I. Absolute and difference spectra. J. Biol. Chem. 235, 845–852.

Zhu, F., Zhang, D., He, Y., Liu, F., Sun, D.-W., 2013. Application of Visible and Near Infrared Hyperspectral Imaging to Differentiate Between Fresh and Frozen–Thawed Fish Fillets. Food Bioprocess Technol. 6, 2931–2937. doi:10.1007/s11947-012-0825-6